ACS APPLIED ENGINEERING MATERIALS

pubs.acs.org/acsaenm Article

Hybrid Mixed-Metal Oxide Latex Composite Thin Films for Passive Control of Indoor Formaldehyde

Peter O. Aina, Busuyi O. Adebayo, Kyle Newport, Ali A. Rownaghi,* and Fateme Rezaei*

Cite This: ACS Appl. Eng. Mater. 2023, 1, 1843−1855 Read Online

ACCESS | Metrics & More | Article Recommendations

ABSTRACT: This study presents the preparation, characterization, and formaldehyde (HCHO) adsorption performance of hybrid mixed-metal oxide (MMO)−coated latex composites for indoor air quality control. The hybrid MMO−latex composites were prepared by coating a thin layer of TiO_2/SiO_2 particles onto a latex polymer film using polypropylene glycol (PPG) to aid in uniform deposition of MMO particles via hydrogen bonding, while also providing additional active sites for HCHO adsorption. The effect of PPG content on the HCHO removal performance of the composites in terms of capture capacity and kinetics were systematically investigated. The indoor chamber tests indicated that the HCHO adsorption capacity and kinetics of the composite thin film increased by 36% and 63%, respectively, compared to those of its MMO-incorporated latex analogue under identical conditions. Moreover, our results indicated that upon increasing the PPG content from 0 to 90 wt %, the HCHO adsorption capacity and rate were significantly enhanced from 0.36 to 0.57 mmol/g and 0.01 to 0.14 h^{-1}, respectively, due to increased affinity and better accessibility to the adsorption active sites in the thin films with uniformly deposited MMO particles. The increase in the humidity level from 45 to 80% RH was also found to promote the rate of HCHO capture by 50%. The findings of this work demonstrate that hybrid MMO−coated latex composites have superior HCHO adsorptive performance compared to their incorporated MMO−latex analogues.

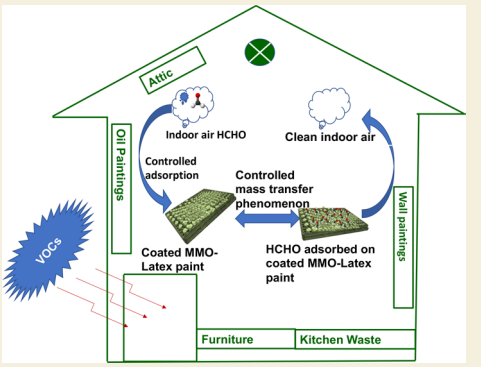

KEYWORDS: *Composite thin film, HCHO removal, Indoor air, Passive control, Latex coating*

1. INTRODUCTION

There is no doubt that the quality of the indoor environment has a significant effect on human health, given that people spend most of their day in indoor settings. The presence of indoor air pollutants such as volatile organic compounds (VOCs) can dramatically affect indoor air quality (IAQ) and hence, human health.[1,2] Among various VOC types, aldehydes emitted by household finishes and associated materials like paints and adhesives can cause serious health concerns, especially when their concentration exceeds the upper recommended limit.[3,4] For example, exposure to a dose of 0.5 mg/m^3 formaldehyde (HCHO) over a prolonged time can lead to airway irritation and rhinitis.[5] Recent studies have shown that indoor HCHO concentration in 70% of newly built apartments exceeded the national standards.[6]

The removal of indoor air pollutants is mainly achieved via air purifiers with absorption media or air conditioning systems (HVAC).[7] Other methods such as botanical filtration,[8] catalytic oxidation,[9] adsorption,[10] and plasma have also been investigated to abate indoor VOCs. Among these approaches, passive abatement of indoor VOCs over sorbent materials offers a promising approach for IAQ control. In this context, various sorbents including activated carbons,[11−14] silicas,[15−18] zeolites,[19,20] metal−organic frameworks (MOFs),[21] and metal oxides[22] have been extensively investigated in indoor settings. Recently, our group explored the use of ZrO_2/SiO_2 and TiO_2/SiO_2 with varied composition in HCHO adsorption and demonstrated the efficacy of these materials for the removal of indoor aldehydes.[23] Other composite materials such as MnO_2/UiO-66 were recently demonstrated to effectively harness the adsorption−catalysis synergy for removal and subsequent oxidation of HCHO.[24] Recent studies have also demonstrated the suitability of composite sorbents as air purifiers to remove trace VOCs from indoor air.[25−27]

A passive abatement approach can offer an efficient removal strategy without increasing the ventilation rate and, consequently, the cost of IAQ management. To passively control indoor pollutants via adsorption method, the sorbent (or catalyst) particles can be incorporated into paint or coated

Received: April 18, 2023
Revised: May 24, 2023
Accepted: May 26, 2023
Published: June 16, 2023

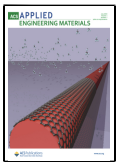

https://doi.org/10.1021/acsaenm.3c00194
ACS Appl. Eng. Mater. 2023, 1, 1843−1855

Scheme 1. Illustration of the Formation of Hybrid MMO-Coated Latex Composite Thin Films

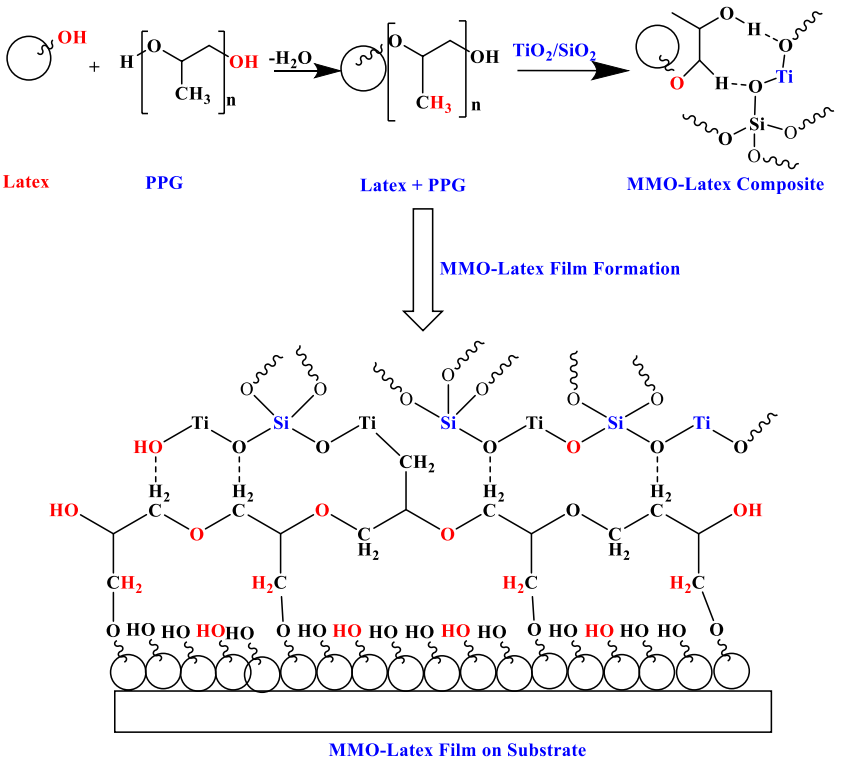

onto the surface to act as a sink for the pollutants. For example, Wang et al.[28] investigated ultrathin MnO_2-coated FeOOH catalyst for indoor HCHO oxidation at ambient temperature and showed that the composite filter could reduce various concentrations of HCHO (150−450 ppb) down to the WHO guideline value (≈ 81 ppb) within 60 min.[28] Our previous work[29] also demonstrated the efficacy of sorbent-incorporated latex paints in abating HCHO vapor at room temperature through a passive method. However, the incorporation of sorbent particles into the latex matrix gave rise to about 30−60% reduction in adsorption capacity and 60−100% decrease in adsorption rate.

To address these issues, we embarked on a study to develop sorbent−latex composites via surface coating approach instead of previously demonstrated matrix incorporation method for indoor HCHO abatement. Our testing hypothesis was that uniform deposition of MMO particles onto the latex surface could minimize the diffusion barriers and pore blockage issues associated with the incorporation method, thereby enhancing both the capture kinetics and the amount. Specifically, in this proof-of-concept study, we report coating of a thin film of TiO_2/SiO_2 onto the surface of the latex polymer with the aid of polypropylene glycol (PPG). The hybrid MMO-coated latex composites were then tested for adsorptive removal of HCHO. This is the first detailed experimental study of HCHO adsorption on hybrid MMO-coated latex composite thin films in the context of indoor air quality control. The effects of hybrid composite preparation conditions, feed concentration, temperature, and relative humidity (RH) level on the HCHO abatement were studied in detail in a closed chamber under passive and active flow conditions. The addition of PPG was done intentionally to strengthen the interaction between TiO_2/SiO_2 particles and the latex polymer, as displayed in Scheme 1. Our working hypothesis was that PPG can not only serve as a binder to form MMO clusters on the surface of the latex polymer, but also provide additional active sites for HCHO adsorption.

2. EXPERIMENTAL SECTION

2.1. Materials

Tetraethyl orthosilicate (TEOS, 98%), titanium(IV) butoxide (TBT, reagent grade, 97%), hexadecyltrimethylammonium bromide (CTAB), and triethanolamine ($TEAH_3$) used in the preparation of the composites, and HCHO solution (ACS reagent, 37% in H_2O) used as the HCHO vapor-generating source in the adsorption experiments were all purchased from Sigma-Aldrich. Cellosize QP 4400, polypropylene glycol, AMP 95, CANGUARD 327, Triton X-100, Byk 22, E-SPERSE 100, Joncryl 1532, and UCAR IBT used in the preparation of the hybrid MMO−coated latex composites were all purchased from commercial vendors. All these chemicals were used as received without any further purification.

2.2. Synthesis of Hybrid MMO-Coated Latex Composites

The hybrid MMO-coated latex (LSP) composites were synthesized by slowly adding 0.095 g of the thickener (Cellosize QP 4400) to the mixture of 1.45 mL of PPG and 11.99 mL of DI water, followed by stirring until a homogeneous mixture was obtained, while maintaining pH of 9.5 by addition of 0.14 mL of AMP-95 to the mixture. Next, CANGUARD-327, Triton X-100, and Byk22 in the amounts 0.095, 0.095, and 0.14 mL, respectively, were added as a defoamer to the solution. A total of 1.17 mL of E-SPERSE 100 was also added as a dispersant in the next step, after which the mixture was dispersed for 30 min, and then 16.33 mL of Joncryl 1531 was added as an emulsifier to the mixture, and finally 0.5 mL of UCAR IBT was added as a film former to complete the latex phase formation. The resultant solution was then spread on a glass disc and allowed to solidify for 6 h. PPG was then added to the surface of the solidified latex, PPG dissolves the late surface and prepares the substrate for subsequent binding with the TiO_2/SiO_2. The TiO_2/SiO_2 particles were sprayed onto the surface of the latex-PPG composite using a powder gun at a low pressure of 20 psi to achieve a uniform thickness across the surface.

https://doi.org/10.1021/acsaenm.3c00194
ACS Appl. Eng. Mater. 2023, 1, 1843−1855

The final form of composite was obtained by exposing and curing the thin film to the heat under vacuum at 35−50 °C for 48−72 h. The samples were labeled LSP-*x*, where *x* indicates the weight composition of PPG in the hybrid composite. The compositions of the synthesized hybrid MMO-coated latex composites are listed in Table 1. In addition to the coated composites, we also prepared TiO_2/SiO_2-incorporated latex (LS) composite as a control material following a procedure reported in our previous work.[29]

Table 1. Composition of Hybrid MMO-Coated Latex Composites

Material	MMO content (wt %)	Latex content (wt %)	PPG content (wt %)
LSP-0	10	90	0
LSP-20	10	70	20
LSP-30	10	60	30
LSP-50	10	40	50
LSP-75	10	15	75
LSP-90	10	0	90

2.3. Characterization of Hybrid MMO-Coated Latex Composites

The textural properties of the hybrid thin film composites were analyzed by N_2 physisorption at 77 K on a 3Flex volumetric gas analyzer (Micromeritics). Before the tests, the samples were degassed at 60 °C for 6 h on a SmartVac Prep system to remove contaminants or water vapor. From the isotherms, the surface area was determined using the linearized Brunauer−Emmett−Teller (BET) model in the relative pressure range of $0.04 < P/P_0 < 0.3$, whereas the density functional theory (DFT)−Hasley thickness model was used to determine pore volume and pore size distribution (PSD). The thermal stability of the composites was investigated via thermogravimetric analysis on a Q-500 (TA Instruments) TGA to probe their applicability as a permanent HCHO trap. Scanning electron microscopy (SEM) was conducted on the materials using a Zeiss Merlin Gemini field emission microscope to assess the surface morphology and the thickness of the thin films. A combination of backscattering microscopy and energy dispersive spectroscopy (EDS) was performed on a Quanta 600F ESEM with a Bruker Quantax EDS to map the dispersion of the oxide phases. Fourier transform infrared (FTIR) spectroscopy was performed on all samples to determine the chemical structure of the composites using Nicolet iS50 Thermoscientific FTIR spectrometer.

2.4. HCHO Adsorption Chamber Tests

The HCHO adsorption experiments were conducted in a controlled environmental test chamber to assess the impact of composite thin films' characteristics on HCHO adsorption capacity and kinetics. The setup was made up of a glass container connected to a cuboidal box inside which an HCHO meter (HalTech, HAL-HFX 205) and a RH meter (AEMC instruments, IAQ meter 1510) were placed for monitoring the concentration of the HCHO at the chamber outlet and the humidity level, respectively. The cuboidal box acted as an insulated environment to maintain the operating conditions. A saturator filled with DI water was used to control the RH of the chamber. A separate saturator was filled with an aqueous HCHO solution, to which air was flown to carry HCHO vapor into the chamber. A bypass run preceded each adsorption run to determine the chamber inlet HCHO concentration. The concentration of the generated HCHO in parts per million volume (ppm_v) was determined from eq 1:[30]

$$c_{gen} = \frac{rF_c}{F_d + (r+1)F_c} \times 10^6 \quad \text{where} \quad r = \frac{P^{sat}_{HCHO}}{P_{in}} \tag{1}$$

In eq 1, c_{gen} (ppm_v) is the concentration of the HCHO vapor generated, F_c (mL/min) and F_d (mL/min) are carrier gas and diluent flow rates, respectively, P_{in} (psig) is the carrier gas chamber inlet pressure, and P^{sat}_{HCHO} (psig) is the HCHO vapor partial pressure of the aqueous solution. The values of F_c and F_d were varied to achieve the desired concentrations (ca. 5, 10, 20 ppm_v). The flow rate of the HCHO stream that entered the chamber was set by a mass flow controller (MFC), while the balance (any unused portion) was vented.

Once HCHO was generated and the concentration was allowed to reach steady state at the desired value, the HCHO/air feed was introduced into the chamber to start the adsorption runs. The flow rate to the chamber was set at 60 mL/min. Adsorption was continued until saturation was attained. The HCHO adsorption capacity was calculated using eq 2:

$$q_{ads} = \frac{F_{in}c_{in}t_{ads}}{24.8 \times m_s} \times 10^{-6} \quad \text{where} \quad t_{ads} = \int_0^{t_{sat}} \left(1 - \frac{c_{out}}{c_{in}}\right) dt \tag{2}$$

where q_{ads} (mmol/g) is the HCHO dynamic adsorption capacity, F_{in} (mL/min) and c_{in} (ppm_v) are the chamber inlet volumetric flow rate and HCHO concentration, respectively, t_{ads} and t_{sat} (min) are the adsorption and saturation times, respectively, 24.8 (mL/mol) is the ideal gas molar volume at 25 °C and 1 atm, and m_s (0.2 g) is the

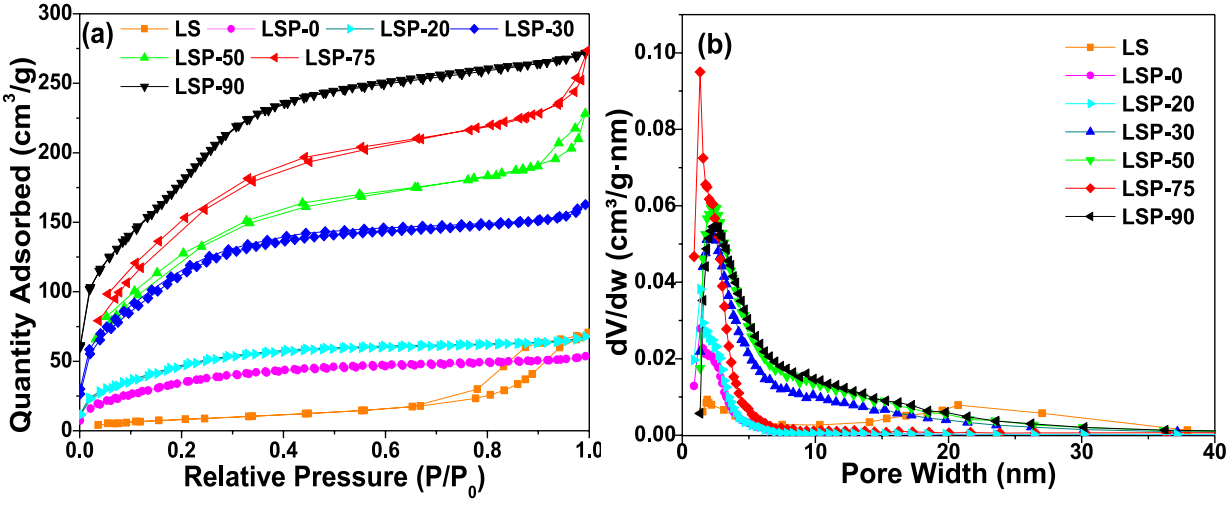

Figure 1. (a) N_2 physisorption isotherms and (b) PSD profiles for hybrid MMO-coated latex composites.

https://doi.org/10.1021/acsaenm.3c00194
ACS Appl. Eng. Mater. 2023, 1, 1843−1855

composite mass. c_{in} is the same as c_{gen} in eq 1, and c_{out} is the concentration inside the chamber.

2.5. Adsorption/Desorption Rate Modeling

To better assess the kinetics of adsorption of HCHO over the hybrid composites, the adsorption rate constant, k_{ads} (h^{-1}), was calculated by fitting the concentration profiles against time in the sink region with a first-order rate model in eqs 3a−3b:

$$\frac{dc_{out}}{dt} = -k_{ads}c_{out} \quad (3a)$$

by integration followed by linearization, we have

$$\ln c_{out} = \ln c_{in} - k_{ads}t \quad (3b)$$

The adsorption rate constants were calculated from the slope of the linear fittings of eq 3b. Similarly, the desorption rate constant, k_{des} (h^{-1}), was estimated from the desorption profiles using the above equations.

3. RESULTS AND DISCUSSIONS

3.1. Hybrid MMO-Coated Latex Composites Characterization

The N_2 physisorption isotherms of the composites are shown in Figure 1. According to the IUPAC classification,[31] the MMO-incorporated composite (LS) exhibited type V isotherms, indicating a poorly developed micropore but mesoporous class of material with weak affinity toward adsorbates. However, the LS sample showed a typical H2 hysteresis, which is similar to what was reported earlier by Adebayo et al.[29] Type H2 corresponds to channels with a pore mouth smaller than the pore body, and its presence indicates the predominant ink-bottle pores. On the other hand, LSP-0, LSP-20, and LSP-30 materials displayed type I−IV isotherms, indicating the presence of both micro-and mesopores in these materials. Furthermore, upon increasing the PPG loading, the hysteresis loop for LSP-50 and LSP-75 became more pronounced, implying the presence of more mesopores, while the H3 hysteresis loop signified the presence of pores created by agglomerated/stacked particles.[32] However, LSP-90 displayed type I isotherms, indicating the presence of primarily micropores in its structure. Nevertheless, the amount of N_2 physisorbed was directly proportional to the amount of the PPG loaded in each sample. The same trends observed in the isotherms were seen in the PSD profiles presented in Figure 1b.

The estimated textural properties of the hybrid MMO-coated latex composites extracted from N_2 physisorption isotherms are summarized in Table 2. The BET surface area and pore volume showed an increasing trend with the PPG content and a decreasing trend with the latex content, with LSP-90 possessing the highest surface area (403 m^2/g) and pore volume (0.30 cm^3/g), which were 7.7 and 3 times larger than those of the LS sample with a surface area of 52 m^2/g and pore volume of 0.01 m^3/g, respectively. This could be due to the reduction in the contact area between the MMO particles and the latex compared to the LS composite. This was expected as one of the drawbacks of the matrix incorporation technique is the porosity/surface area reduction due to a full contact between the MMO particles and the polymer matrix. It is also worth noting here that the pores of the composites fell in the range of 1−3 nm.

Table 2. Textural Properties of Hybrid MMO-Coated Latex Composites

Materials	S_{BET} (m^2/g)	V_{micro} (cm^3/g)	V_{meso} (cm^3/g)	d_p (nm)
LS	52	0.00	0.08	3
LSP-0	130	0.01	0.10	1, 2
LSP-20	160	0.02	0.11	1, 2
LSP-30	330	0.03	0.33	2, 3
LSP-50	359	0.09	0.35	1, 2
LSP-75	372	0.07	0.31	1, 3
LSP-90	403	0.14	0.30	1

The TGA profiles in Figure 2 showed different weight losses at different temperatures, which arose from the components of the hybrid MMO-coated latex composites. The first weight loss below 100 °C corresponded to 9% of the total weight of the samples and was attributed to the volatilization of low boiling point components. The second weight loss (7%) between 100 and 250 °C was responsible for the desorption of the physisorbed water molecules on the surface of the material. The most prevalent weight loss (ca. 60−70%) was observed in the temperature range of 350−450 °C, which was attributed to the decomposition of the latex polymer. The nonvolatile residue (10%) corresponded mainly to the inorganic content of the samples (TiO_2/SiO_2), which was similar for almost all the samples due to the same amount of MMO used in their synthesis.

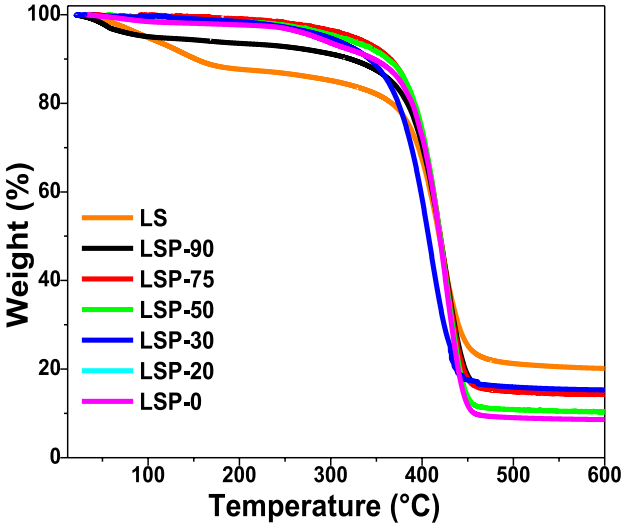

Figure 2. Thermogravimetric analysis of the hybrid MMO-coated latex composites.

The developed materials were also characterized by FTIR to determine any changes in the chemical structure of the polymer after MMO coating and PPG functionalization. Figure 3 depicts the FTIR spectra of the bare latex with different compositions of PPG (i.e., LP-*x* samples) and MMO-coated latex composites (LSP-*x* samples). To identify the role of PPG in the formulation and binding of MMO to the surface of the latex paint, the FTIR spectrum of the liquid latex was also taken before adding PPG. As evident from Figure 3a, the intensity of the C−H peak at 2950 cm^{-1} increased with increasing the PPG content, whereas the O−H peak intensity at 3400 cm^{-1} decreased due to the solidification of this material. Such a trend demonstrates the reduction in intramolecular hydrogen bonding that makes the C−H groups readily available for intermolecular bonding. The presence of C−H functional groups in LP-*x* confirms the possibility of

https://doi.org/10.1021/acsaenm.3c00194
ACS Appl. Eng. Mater. 2023, 1, 1843−1855

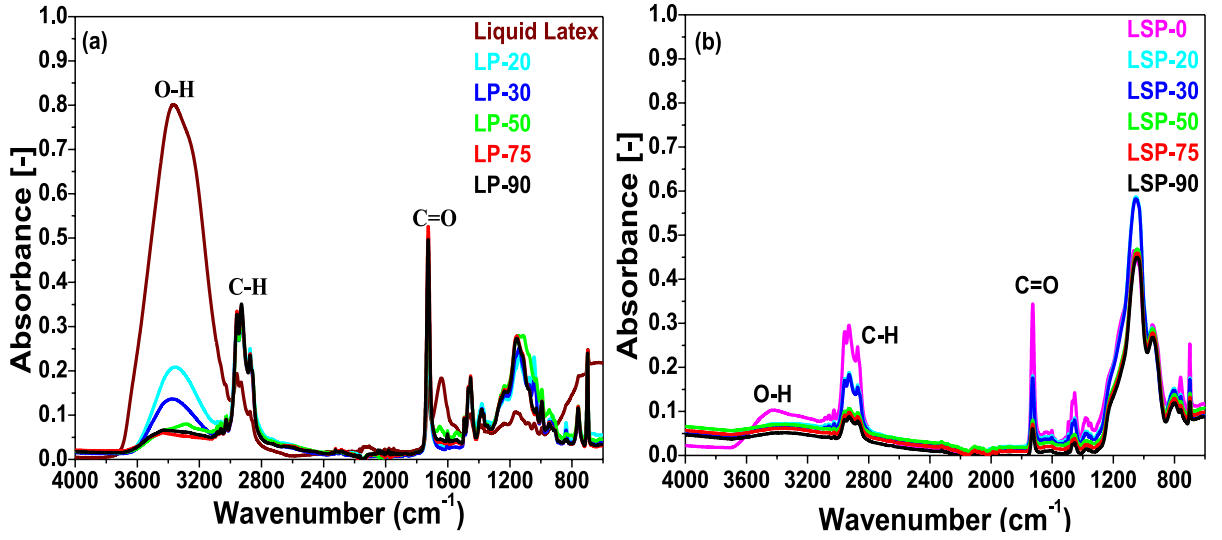

Figure 3. FTIR spectra of (a) bare latex with different compositions of PPG and (b) MMO-coated latex composites.

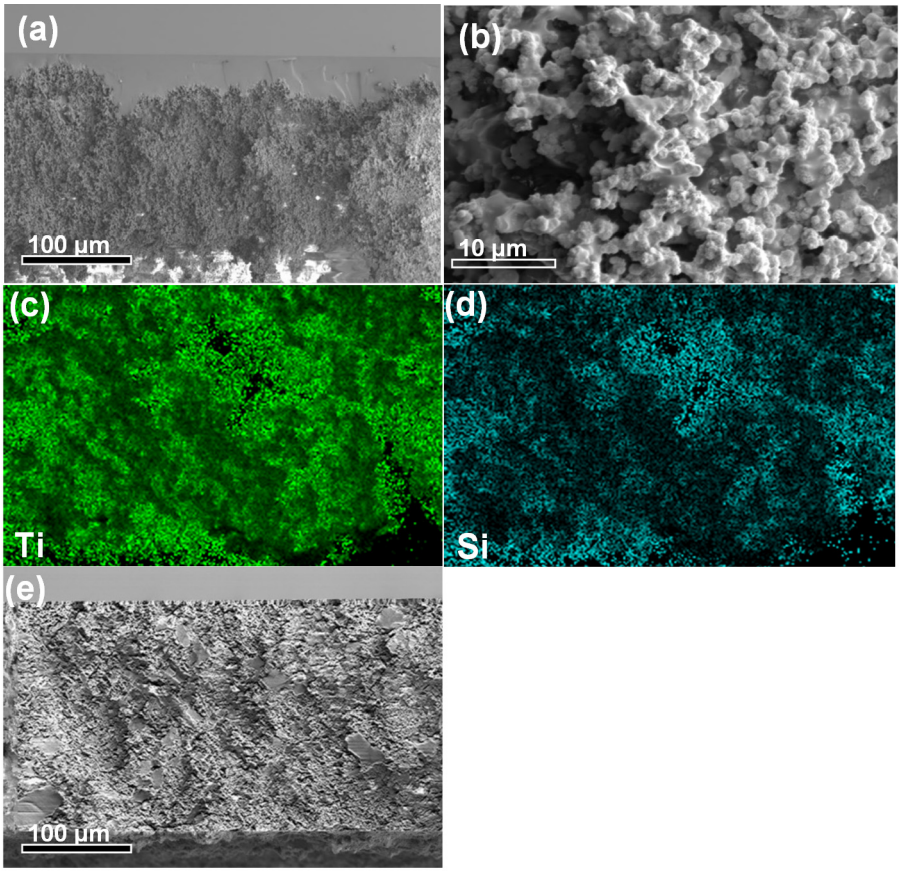

Figure 4. SEM images of MMO-coated latex composites: (a) lateral view and (b) aerial view; EDS of (c) Si and (d) Ti elements; and SEM image of (e) MMO-incorporated latex composite.

hydrogen bonding between the substrate and the MMO. On the contrary, for the LSP-*x* samples (Figure 3b), a decrease in the peak intensity of the C−H stretching vibration and broadening of the hydroxyl peaks was observed, which further confirmed the occurrence of hydrogen bonding, as broadening of the O−H peak has been ascribed to the presence of hydrogen bonding.[33,34] Conversely, the reduction in the absorbance of the C−H peak could be attributed to the utilization of this C−H band in binding with MMO.

The surface morphology of the MMO-coated latex composites was assessed by SEM, and the corresponding images of LS and LSP-50 samples are presented in Figure 4. The lateral view in Figure 4a shows the uniform distribution of the TiO_2/SiO_2 MMO particles on the polymer surface, whereas the aerial view in Figure 4b reveals the size of the particles falling in the range of 5−10 nm. This image also reveals the deposited film's porous nature and confirms that the particles were held tightly together by the binder (i.e.,

https://doi.org/10.1021/acsaenm.3c00194
ACS Appl. Eng. Mater. 2023, 1, 1843−1855

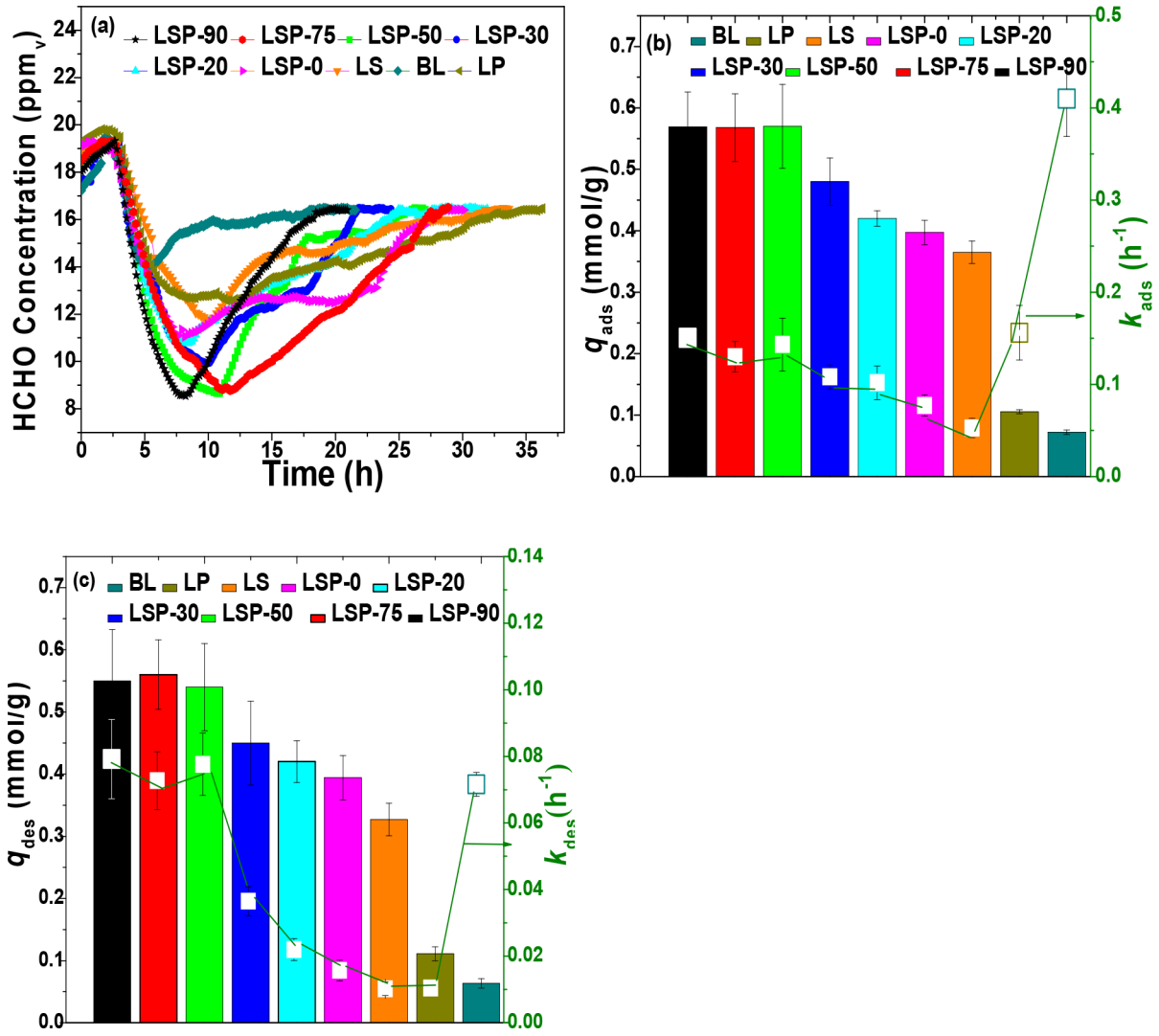

Figure 5. (a) Concentration profiles of HCHO over hybrid MMO-coated latex composites during adsorption and desorption, (b) the corresponding adsorption capacities and rates, and (c) the corresponding desorption capacities and rates. Experimental conditions: 20 ppm$_v$, 25 °C, and 45% RH.

PPG). Despite their small size and low loading, the deposited MMO particles can be observed on the latex surface, however, it should be noted here that the thickness of the coated MMO film was not quite uniform and that some chunks of the agglomerated particles sunk into the latex substrate to provide a root for the top layer.[35] Overall, these SEM images confirm that the MMO particles were not buried inside the latex, and there was a distinct layer between the latex and the deposited layer. To confirm the presence of Ti/Si within the MMO-coated latex composite as well as successful integration of MMO with the solid latex support, the EDS images were collected (Figure 4c,d). These images depict the elemental mapping of Ti and Si within the MMO film and provide direct evidence for uniform distribution of TiO_2/SiO_2 over the surface. They also hint at partial agglomeration of the particles, yet the film provides a porous pathway for diffusion of vapor molecules. To have a basis for comparison, we also assessed the morphology of the MMO-incorporated latex composite. Figure 4e shows the uniform distribution of the MMO particles within the polymer matrix. Notably, the size of the particles was found to be comparable to those shown in the coated analogues.

3.2. HCHO Adsorption Chamber Tests

First, the effect of PPG loading on the capture performance of the hybrid MMO-coated latex composites was investigated. Shown in Figure 5 are the HCHO concentration profiles obtained from the chamber tests at 25 °C, 45% RH, and 20 ppm$_v$. The bare-latex (BL) profile was also included as a control material. The effectiveness of both sets of composites (i.e., MMO-incorporated (LS) and MMO-coated (LSP)) in passively mitigating HCHO was characterized by the sloppy sink in the concentration profile when compared to that of the bare latex, followed by desorption that led to a gradual rise in the HCHO concentration after HCHO saturation. As shown in Figure 5, a drop in the chamber's HCHO concentration was observed after the initial steady-state period due to HCHO adsorption on the composites. For the BL sample, the concentration was reduced to only ~15 ppm$_v$. This slight reduction in HCHO concentration observed in the concentration profile of BL could be linked to the interactions between the hydroxyl groups in the latex and hydrogen groups in HCHO.[36] The underlying mechanism that explains the adsorptive performance of LP-*x* materials is similar to that of the BL except for the accompanied reversible chemical reaction

https://doi.org/10.1021/acsaenm.3c00194
ACS Appl. Eng. Mater. 2023, 1, 1843−1855

between the PPG and HCHO to form hemiacetal and finally acetal when heat is being applied, as explained by Broekhuis et al.,[37] and schematically depicted in Scheme 2.

Scheme 2. Schematic Showing the Role of Polypropylene Glycol in Promoting HCHO Adsorption

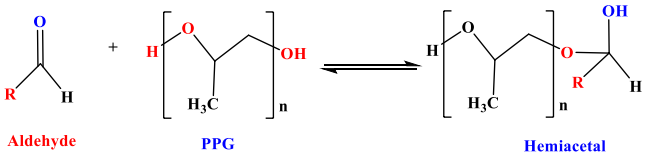

On the other hand, the combined effects of physisorption over MMO particles and the chemical interactions with the hydroxyl groups of PPG gave rise to a superior performance for the LSP materials over their LP analogues. The acidic properties of TiO_2/SiO_2 particles promote the amount of surface OH^- groups, thereby contributing to higher affinity toward HCHO. The previously explained premises demonstrated the trend of the results shown in Figure 5a as the drop in the HCHO concentration level was found to be in the order of LSP-90 (8.3 ppm_v) ~ LSP-75 (8.4 ppm_v) > LSP-50 (8.5 ppm_v) > LSP-30 (10.3 ppm_v) > LSP-20 (10.8 ppm_v) > LSP-0 (11.0 ppm_v) > LS (11.5 ppm_v) > LP (13.0 ppm_v).

Shown in Figure 5b,c are the calculated adsorption and desorption capacities (q_{ads} and q_{des}, respectively) along with the corresponding adsorption and desorption rate constants (k_{ads} and k_{des}) for the chamber tests ran at 20 ppm_v, 25 °C, and 45% RH. The LSP-50 exhibitted the highest adsorption capacity at 0.57 mmol/g at a rate of 0.14 h^{-1}, which were 36% and 63% higher than those for the MMO-incorporated counterpart (LS) sample, respectively. The addition of PPG was found to have a positive effect on the HCHO abatement performance of the latex composite. For example, q_{ads} increased from 0.36 mmol/g for LSP-0 to 0.57 mmol/g for LSP-50. It was also noticed that the improvement in the adsorption performance is directly proportional to the amount of PPG loaded up to 50 wt %, which emphasizes the importance of a balanced amount of chemisorption- and physisorption-based material to achieve maximum adsorption capacity. Similarly, comparing the desorption properties of the composite materials in Figure 5c, the desorption rate and capacity increased with the amount of PPG loaded across all materials. This trend can be associated with the reversible phenomenon described in Scheme 2, as the moisture content in the chamber reduced with the PPG content. The results shown herein also followed the expected trend as revealed from the FTIR analysis that the degree of adhesion between MMO particles and the latex polymer increases with PPG content up to 50 wt %.[36,38]

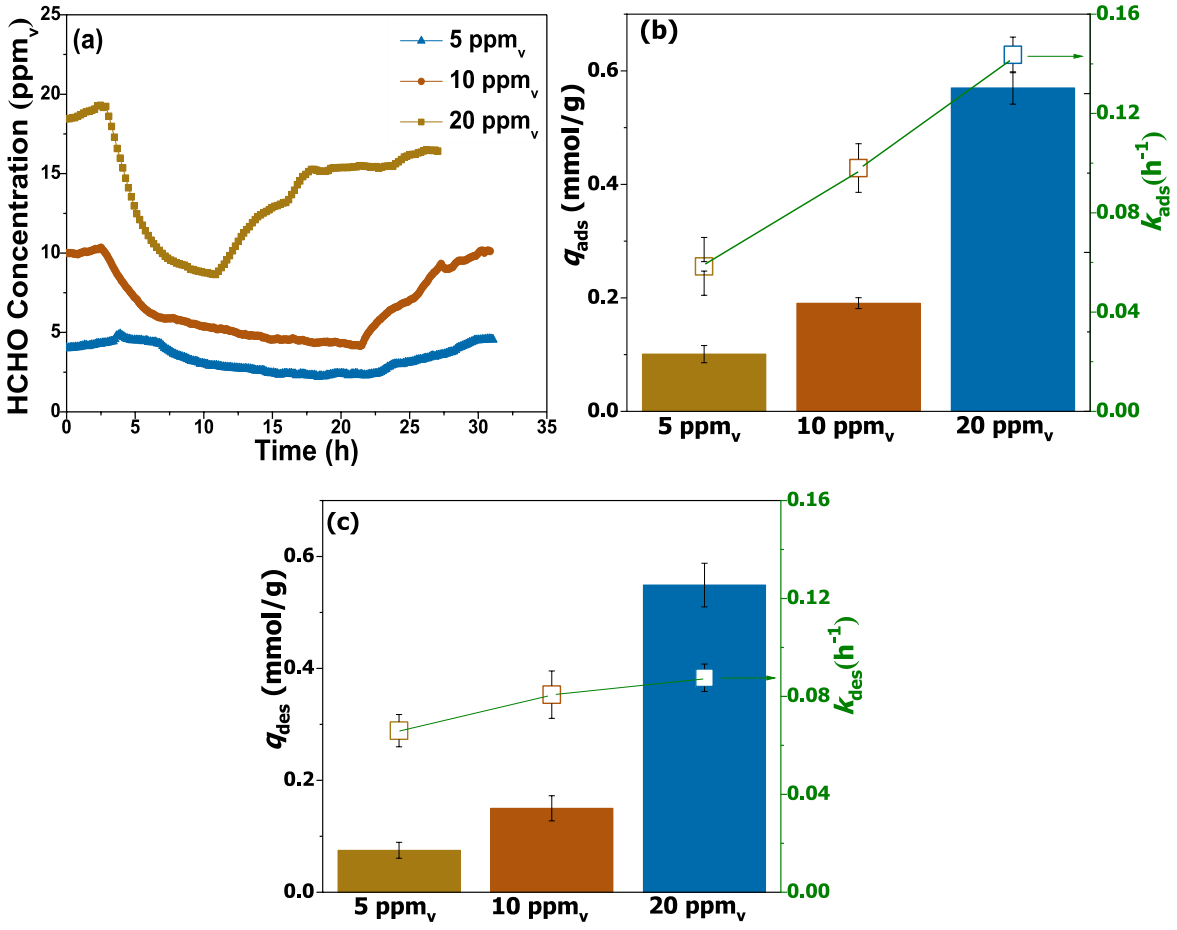

Figure 6. (a) Adsorption profiles of LSP-50 at 5, 10, and 20 ppm_v, (b) the corresponding adsorption capacities and rate constants, and (c) the corresponding desorption capacities and rate constants: bar chart for q_{ads}, q_{des} and line graph for k_{ads}, k_{des}. Experimental conditions: 25 °C and 45% RH.

https://doi.org/10.1021/acsaenm.3c00194
ACS Appl. Eng. Mater. 2023, 1, 1843−1855

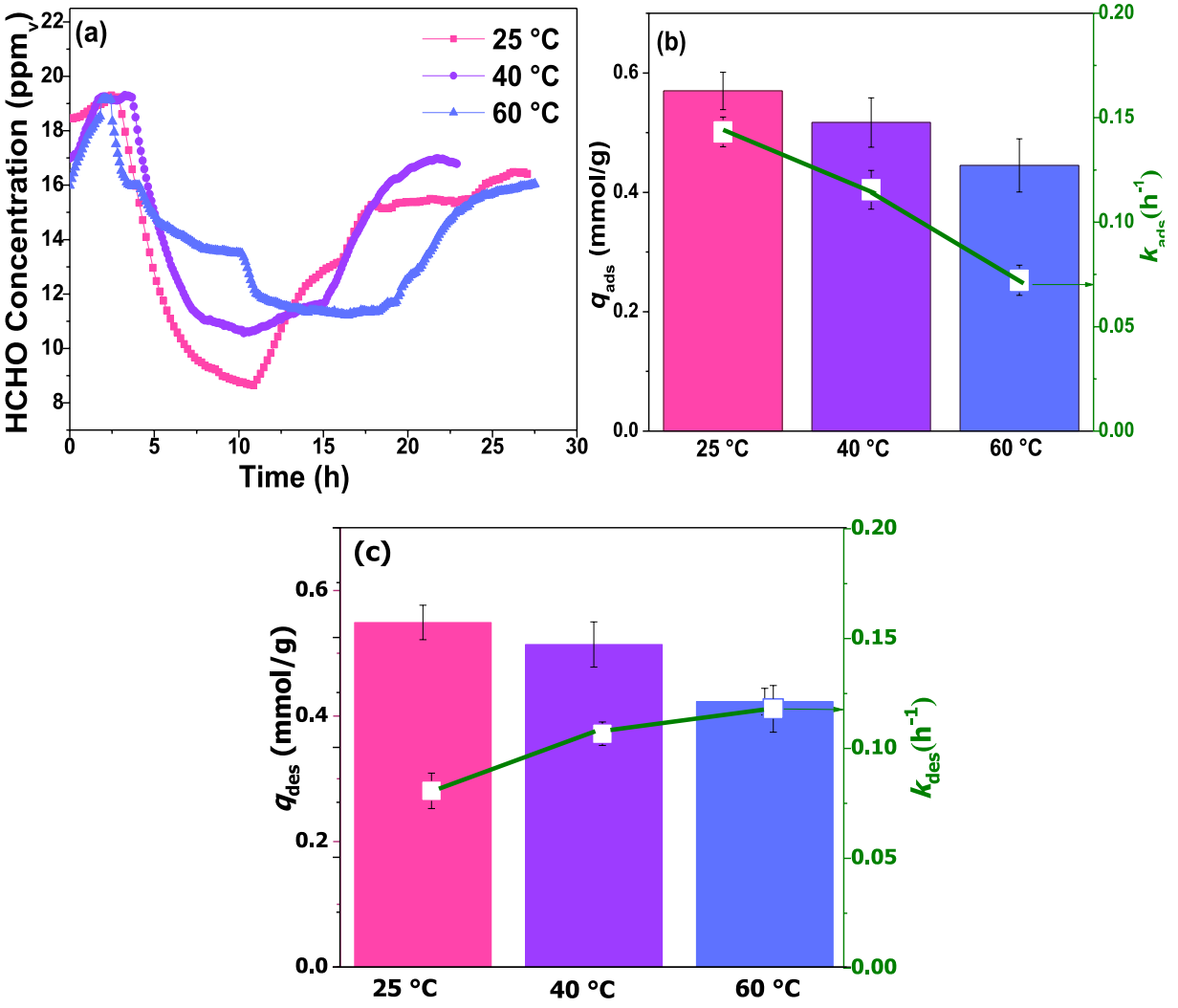

Figure 7. (a) Adsorption profiles of LSP-50 at 25, 40, and 60 °C, (b) the corresponding adsorption capacities and rate constants, and (c) the corresponding desorption capacities and rate constants: bar chart for q_{ads}, q_{des} and line graph for k_{ads}, k_{des}. Experimental conditions: 20 ppm$_v$ HCHO and 45% RH.

3.2.1. Effect of Feed Concentration. In the next step, the effect of HCHO feed concentration on capture capacity and rate was explored. The moderation in the ratio of PPG to MMO/latex employed in the preparation of LSP-50 coupled with the superior HCHO abatement performance demonstrated in Figure 5 led us to choose LSP-50 for further analysis. Figure 6 compares the HCHO concentration profiles of the selected material at 5, 10, and 20 ppm$_v$, 25 °C, and 45% RH. According to these results, both adsorption capacity and rate were increased with concentration, in agreement with the reported data in the literature.[36,38] However, as inlet concentration increased from 5 to 20 ppm$_v$, the saturation time was shortened from ∼15 to 7 h. Given the ultradilute (i.e., sub-ppb-level) concentration of the aldehydes in indoor environments, the time to reach full saturation will be significantly longer (e.g., on the order of months or even years) than what was found here. As shown in Figure 6b, the adsorption rates estimated during the HCHO sink were 0.06, 0.10, and 0.14 h^{-1} at 5, 10, and 20 ppm$_v$, respectively, whereas the corresponding adsorption capacities were found to be 0.1, 0.2, and 0.57 mmol/g. The corresponding desorption capacities and rates exhibited a similar trend to the adsorption properties, as can be observed in Figure 6c. In particular, at 5 ppm$_v$, the q_{des} and k_{des} values for LSP-50 were estimated to be 0.075 mmol/g and 0.06 h^{-1}, respectively, whereas at 10 ppm$_v$, the values were found to be 0.15 mmol/g and 0.08 h^{-1}, respectively. Overall, the desorption capacities at three different concentrations were relatively close to their adsorption capacities; however, due to the chemical interactions involved in the adsorption process, the desorption rates were about 50% lower than the adsorption rates.

3.2.2. Effect of Capture Temperature. At a fixed inlet concentration (20 ppm$_v$) and chamber humidity (45% RH), the effect of temperature on the HCHO removal performance of the LSP-50 composite was also assessed, as demonstrated in Figure 7. Expectedly, both adsorption capacity and rate were reduced at higher temperatures, in agreement with the reported studies in the literature.[33,36] This trend was significantly more pronounced during the initial hours when reduction in HCHO concentration took much longer and dropped to ∼11.5 ppm$_v$ at 60 °C and to ∼10 ppm$_v$ at 40 °C, as opposed to ∼8.0 ppm$_v$ at 25 °C. Using the slope of the profiles

https://doi.org/10.1021/acsaenm.3c00194
ACS Appl. Eng. Mater. 2023, 1, 1843−1855

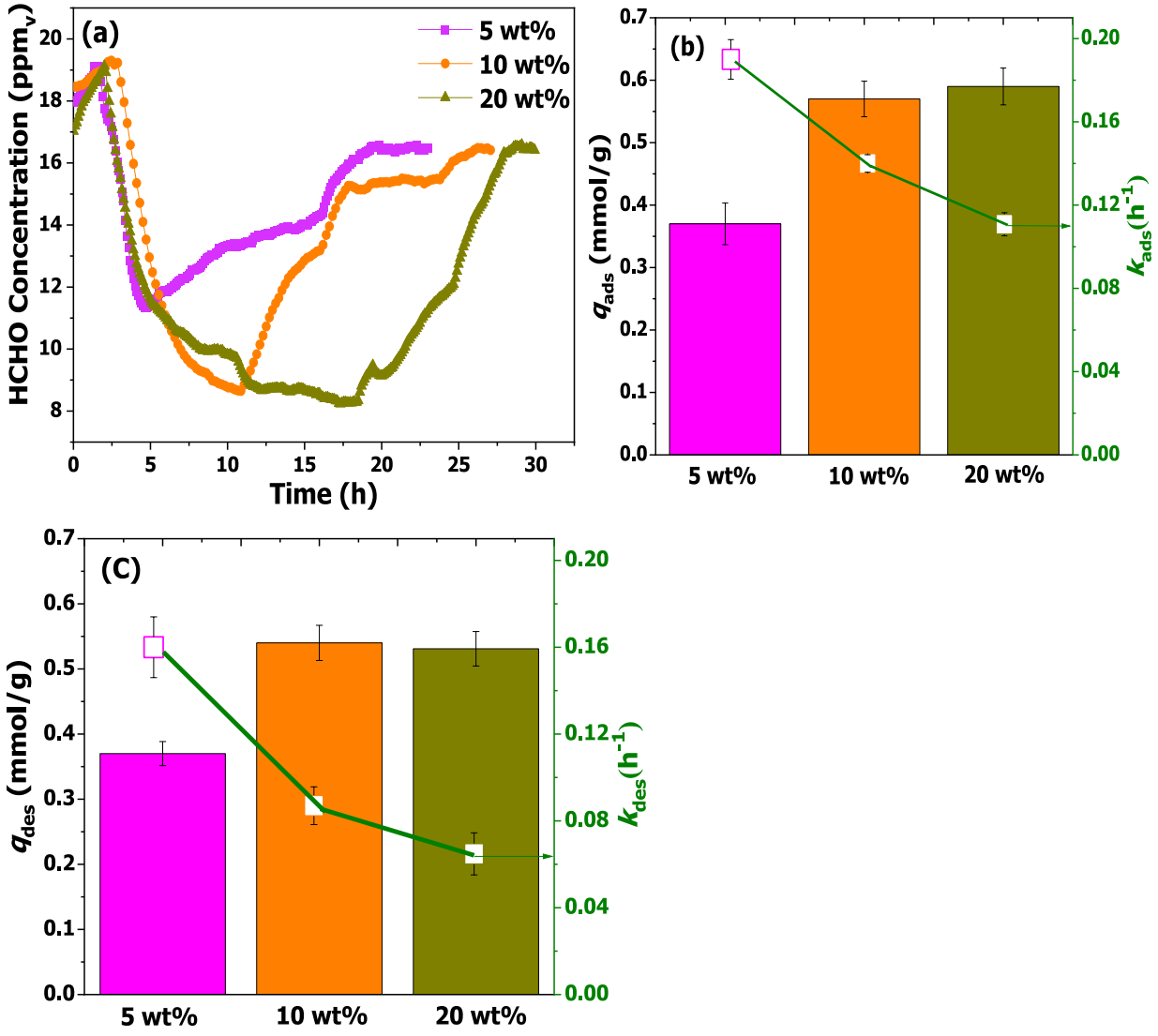

Figure 8. (a) Adsorption profiles of LSP-50 at 5, 10, and 20 wt % MMO loading, (b) the corresponding adsorption capacities and rate constants, and (c) the corresponding desorption capacities and rate constants: bar chart for q_{ads}, $q_{des}$and line graph for k_{ads}, k_{des}. Experimental conditions: 20 ppm$_v$ and 45% RH.

during the HCHO sink, the adsorption rates at 25 and 40 °C were estimated to be about 0.57 and 0.52 h^{-1}, respectively. Accordingly, while full saturation was attained after 15 h at 60 °C, it took about 10 h for the composite to reach its equilibrium capacity at 25 °C under the same conditions. From the thermodynamics standpoint, adsorption being an exothermic reaction involves the release of heat into the surroundings, which will in turn cause reduction in adsorption capacity. In other words, the adsorption and desorption capacities were decreased by as much as 50% as the temperature was increased from 25 to 60 °C. It should, however, be pointed out here that even at elevated temperatures, the composite was still effective in trapping HCHO, but at a slower rate, which is an important consideration given the variation in indoor temperature in commercial or residential buildings, especially across various seasons. These findings are in agreement with the literature reports.[39] Moreover, the desorption rates and capacities of LSP-50 at 25, 40, and 60 °C are shown in Figure 7c. As can be seen, the desorption capacities across the three different temperatures were similar to the corresponding adsorption capacities, while the desorption rates were 30% lower than the adsorption rates. Nevertheless, the desorption rate increased with temperature due to the increase in the HCHO molecules' kinetic energies, as reported in the literature.[40−42]

3.2.3. Effect of Hybrid MMO-Coated Latex Composition. In the next step, the effect of the MMO content on the removal performance of the LSP-50 was assessed by varying the loading from 5 to 20 wt %, while keeping the inlet composition, chamber temperature, and humidity level fixed at 20 ppm$_v$, 25 °C, and 45% RH, respectively, as illustrated in Figure 8. Notably, adsorption capacity increased from 0.37 to 0.59 mmol/g upon increasing the MMO loading from 5 to 20 wt %, but at the expense of a slower rate. However, the adsorption rate and capacity were relatively the same for the 10 and 20 wt % samples, which could be attributed to the particle agglomeration at higher loadings.[43,44] Such effects can not only decrease the accessibility of the available active sites but also add additional barriers to the transport of vapor molecules due to reduction of porosity and blockage of diffusion pathways.[45,46] Hence, the optimum MMO-loading was chosen to

https://doi.org/10.1021/acsaenm.3c00194
ACS Appl. Eng. Mater. 2023, 1, 1843−1855

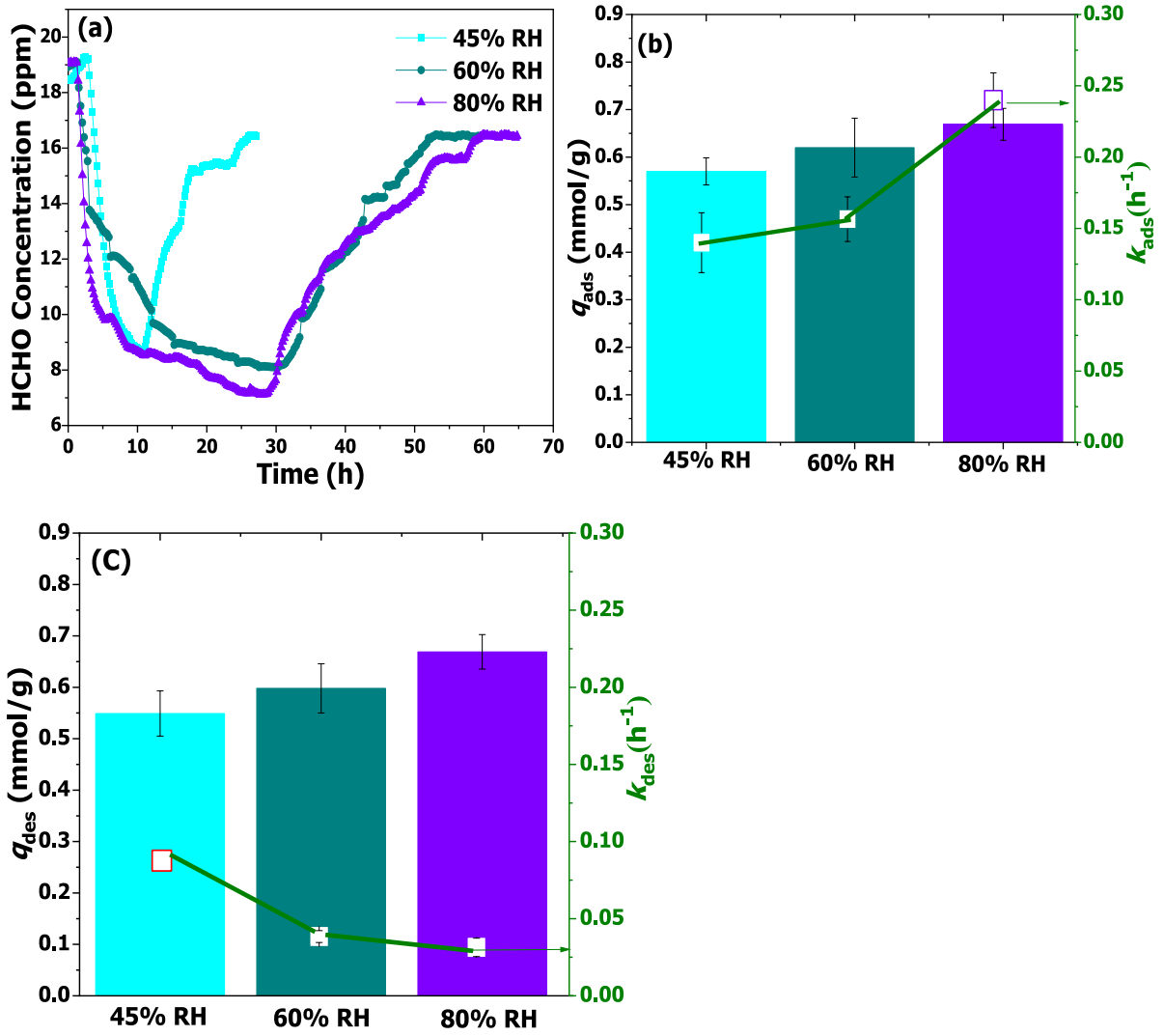

Figure 9. (a) Adsorption profiles of LSP-50 at 45, 60, and 80% RH, (b) the corresponding adsorption capacities and rate constants, and (c) the corresponding desorption capacities and rate constants: bar chart for q_{ads}, $q_{des}$and line graph for k_{ads}, k_{des}. Experimental conditions: 20 ppm_v and 25 °C.

be 10 wt % for the hybrid MMO-coated latex materials. The corresponding desorption rate and capacity values depicted in Figure 8c quantitaively demonstrate the effect of MMO particles agglomeration on desorption properties of LSP-50. While q_{des} increased with MMO loading, k_{des} showed a decreasing trend as a result of lower accessibility to the active sites caused by a higher degree of particles agglomeration. The results presented here are in accordance with the effect of aggregation on the desorption of nanosized zerovalent iron via polymeric surface modifiers according to Kim et al.[47] Similarly, Wang et al.[48] explained how overloaded PEI molecules in PEI/SBA-15 reduce the desorption rate of CO_2.

3.2.4. Effect of Relative Humidity. In the last step of our study, we explored the effect of indoor air humidity on the HCHO removal performance of the LSP-50 composite by conducting the chamber tests at 45, 60, and 80% RH, while keeping the inlet concentration and temperature fixed at 20 ppm_v and 25 °C, respectively. The corresponding HCHO concentration profiles are presented in Figure 9. According to these results, on increasing the RH from 45 to 60 and 80%, the adsorption capacity was slightly increased from 0.57 mmol/g to 0.62 and 0.67 mmol/g, respectively, while the adsorption rate increased from 0.14 to 0.24 h^{-1}. The slight increase in HCHO uptake can be correlated to the water vapor preventing the temperature rise upon HCHO adsorption. On the other hand, a higher level of humidity can further promote the adsorption of HCHO molecules due to the polar nature of the HCHO. The so-called water is essentially a monolayer of OH^- groups bound to the silicon and titanium atoms on the Si/Ti MMO surface.[31,49] These OH^- groups have been proven to be one of the main active sites for adsorption of polar molecules on metal oxides via hydrogen bonding.[49] The calculated desorption capacities and rates at 45, 60, and 80% RH are also depicted in Figure 9c. The desorption capacities and rates reported are quite smaller than the corresponding adsorption values at elevated humidity levels, primarily because of increased adsorbate−adsorbent interactions due to an increase in the concentration of surface OH^-. However, an increase in the concentration of the surface OH^- beyond 60% proved to be relatively insignificant in the desorption of HCHO. Choi et al.[50] used the effective moisture penetration depth (EMPD) model to explain how humidity as a driving force increases the

https://doi.org/10.1021/acsaenm.3c00194
ACS Appl. Eng. Mater. 2023, 1, 1843−1855

adsorption capacity from a thermodynamic perspective. Increasing the RH level also helps to drop the temperature of the surroundings which in turn favors adsorption and decreases desorption until the effect of dry air mass transfer is equal to or greater than the concentration of moisture available within the chamber. Similar results were reported by Liu et al.[45] when toluene was passed over a bed of vaseline loaded-graphite adsorbent under 60 and 80% RH. In the 80% RH runs, a lower desorption rate was attained compared to the 60% RH case, which was attributed to the negative effect of excess water molecules adsorbed on the surface, thereby leading to the formation of polarized groups on the surface of the graphite.

3.2.5. HCHO Adsorptive Performance Comparison. To demonstrate the efficacy of our best performing material, we compared LSP-50 with some of the outstanding polymer/MMO composites reported in the literature. Nomura and Jones[51] synthesized one of the first generations of aminosilica composites for HCHO adsorption and reported a high adsorption capacity of 5.7 mmol/g. In another study, a polyaniline/TiO_2 composite synthesized by Zhu et al.[52] exhibitted an adsorption capacity of 0.67 mg/g when exposed to 0.5 ppm_v of HCHO. Yang et al.[53] synthesized a biodegradable chitosan grafted within β-cyclodextrin to capture gaseous HCHO at room temperature and demonstrated a high adsorption capacity at 15.5 mg/g for this material. In another study, Cu−Mg oxide grafted within an organic polymer was evaluated for adsorption of HCHO and an adsorption capacity of 0.03 mmol/g was reported for this material.[54] Overall, although the HCHO adsorptive performance of LSP-50 appears to be inferior to some of the adsorbents discussed, this composite material outperforms other polymeric composites and emerges as a competitive material to combat the problem of HCHO pollution in indoor air.

4. CONCLUSION

In this study, we reported the first generation of hybrid MMO-coated latex composites for passive abatement of indoor pollutant HCHO as a model VOC compound. Our chamber results revealed that the MMO-coated latex composites outperformed their MMO-incorporated analogues by exhibiting higher HCHO adsorption capacity and kinetics. It was also found that incorporation of the polypropylene glycol up to 50 wt % enhances the removal performance of the composites, with LSP-50 showing the best performance at 0.57 mmol/g capacity and 0.14 h^{-1} adsorption rate at 20 ppm_v inlet concentration, 25 °C chamber temperature, and 45% RH. Furthermore, assessing the effects of temperature and relative humidity revealed that abatement of HCHO is highly favorable at room temperature and a relative humidity of 80%. The HCHO adsorption capacity of LSP-50 under these conditions was recorded to be 0.67 mmol/g at the rate of 0.24 h^{-1}. Overall, this work provides insight into the potential applicability of the surface coating as a suitable, efficient, and cost-effective technique for preparing functional materials for passive abatement of indoor pollutants and thereby, improving the indoor air quality without the need for excessive ventilation rates.

AUTHOR INFORMATION

Corresponding Authors

Fateme Rezaei − *Linda and Bipin Doshi Department of Chemical and Biochemical Engineering, Missouri University of Science and Technology, Rolla, Missouri 65409-1230, United States;* orcid.org/0000-0002-4214-4235; Email: rezaeif@mst.edu

Ali A. Rownaghi − *Department of Chemistry, Cleveland State University, Cleveland, Ohio 44115, United States;* orcid.org/0000-0001-5228-5624; Email: a.rownaghia@csuohio.edu

Authors

Peter O. Aina − *Linda and Bipin Doshi Department of Chemical and Biochemical Engineering, Missouri University of Science and Technology, Rolla, Missouri 65409-1230, United States*

Busuyi O. Adebayo − *Linda and Bipin Doshi Department of Chemical and Biochemical Engineering, Missouri University of Science and Technology, Rolla, Missouri 65409-1230, United States*

Kyle Newport − *Linda and Bipin Doshi Department of Chemical and Biochemical Engineering, Missouri University of Science and Technology, Rolla, Missouri 65409-1230, United States*

Complete contact information is available at: https://pubs.acs.org/10.1021/acsaenm.3c00194

Notes

The authors declare no competing financial interest.

ACKNOWLEDGMENTS

The involvement of A.A.R. in this work was sponsored by the National Science Foundation (NSF CBET-2019350).

REFERENCES

(1) Yu, C. W. F.; Kim, J. T. Long-Term Impact of Formaldehyde and VOC Emissions from Wood-Based Products on Indoor Environments; and Issues with Recycled Products. *Indoor and Built Environment* **2012**, *21* (1), 137−149.

(2) Zhou, X.; Yan, Z.; Zhou, X.; Wang, C.; Liu, H.; Zhou, H. An Assessment of Volatile Organic Compounds Pollutant Emissions from Wood Materials: A Review. *Chemosphere* **2022**, *308*, No. 136460.

(3) Salthammer, T. Formaldehyde Sources, Formaldehyde Concentrations and Air Exchange Rates in European Housings. *Build Environ* **2019**, *150*, 219−232.

(4) Pickrell, J. A.; Griffis, L. C.; Mokler, B. v; Kanapilly, G. M.; Hobbs, C. H. Formaldehyde Release from Selected Consumer Products: Influence of Chamber Loading, Multiple Products, Relative Humidity, and Temperature. *Environ. Sci. Technol.* **1984**, *18* (9), 682−686.

(5) Pazdrak, K.; Górski, P.; Krakowiak, A.; Ruta, U. Changes in Nasal Lavage Fluid Due to Formaldehyde Inhalation. *Int. Arch Occup Environ. Health* **1993**, *64* (7), 515−519.

(6) Liang, W.; Yang, S.; Yang, X. Long-Term Formaldehyde Emissions from Medium-Density Fiberboard in a Full-Scale Experimental Room: Emission Characteristics and the Effects of Temperature and Humidity. *Environ. Sci. Technol.* **2015**, *49* (17), 10349−10356.

(7) U.S. DoE. *Buildings Energy Data Book*. Energy Efficiency & Renewable Energy Department: 2011; Vol. *286*.

(8) Zhang, L.; Routsong, R.; Strand, S. E. Greatly Enhanced Removal of Volatile Organic Carcinogens by a Genetically Modified Houseplant, Pothos Ivy (Epipremnum Aureum) Expressing the

Mammalian Cytochrome P450 2e1 Gene. *Environ. Sci. Technol.* **2019**, *53* (1), 325−331.
(9) Zhang, J.; Shan, R.; Xiao, H.; Hu, S.; Sheng, Z.; Qin, X.; Zhang, Y.; Wang, L.; Li, J.; Zhang, C. Electronic Modification by Transitional Metal Dopants to Tune the Oxidation Activity of Pt-CeO_2-Based Catalysts. *Environ. Sci. Technol.* **2022**, *56* (23), 17331−17340.
(10) Li, H.; Ho, W.; Cao, J.; Park, D.; Lee, S.; Huang, Y. Active Complexes on Engineered Crystal Facets of MnO_x−CeO_2 and Scale-Up Demonstration on an Air Cleaner for Indoor Formaldehyde Removal. *Environ. Sci. Technol.* **2019**, *53* (18), 10906−10916.
(11) Bellat, J.-P.; Bezverkhyy, I.; Weber, G.; Royer, S.; Averlant, R.; Giraudon, J.-M.; Lamonier, J.-F. Capture of Formaldehyde by Adsorption on Nanoporous Materials. *J. Hazard Mater.* **2015**, *300*, 711−717.
(12) Tanada, S.; Kawasaki, N.; Nakamura, T.; Araki, M.; Isomura, M. Removal of Formaldehyde by Activated Carbons Containing Amino Groups. *J. Colloid Interface Sci.* **1999**, *214* (1), 106−108.
(13) Song, Y.; Qiao, W.; Yoon, S.; Mochida, I.; Guo, Q.; Liu, L. Removal of Formaldehyde at Low Concentration Using Various Activated Carbon Fibers. *J. Appl. Polym. Sci.* **2007**, *106* (4), 2151−2157.
(14) Chen, Q.; Liu, F.; Mo, J. Vertical Macro-Channel Modification of a Flexible Adsorption Board with in-Situ Thermal Regeneration for Indoor Gas Purification to Increase Effective Adsorption Capacity. *Environ. Res.* **2021**, *192*, 110218.
(15) Srisuda, S.; Virote, B. Adsorption of Formaldehyde Vapor by Amine-Functionalized Mesoporous Silica Materials. *Journal of Environmental Sciences* **2008**, *20* (3), 379−384.
(16) Lawson, S.; Al-Naddaf, Q.; Krishnamurthy, A.; Amour, M. S.; Griffin, C.; Rownaghi, A. A.; Knox, J. C.; Rezaei, F. UTSA-16 Growth within 3D-Printed Co-Kaolin Monoliths with High Selectivity for CO_2/CH_4, CO_2/N_2, and CO_2/H_2 Separation. *ACS Appl. Mater. Interfaces* **2018**, *10* (22), 19076−19086.
(17) Xu, Y.; Jin, S.; Xu, H.; Nagai, A.; Jiang, D. Conjugated Microporous Polymers: Design, Synthesis and Application. *Chem. Soc. Rev.* **2013**, *42* (20), 8012−8031.
(18) Busca, G.; Lamotte, J.; Lavalley, J. C.; Lorenzelli, V. FT-IR Study of the Adsorption and Transformation of Formaldehyde on Oxide Surfaces. *J. Am. Chem. Soc.* **1987**, *109* (17), 5197−5202.
(19) Bellat, J.-P.; Weber, G.; Bezverkhyy, I.; Lamonier, J.-F. Selective Adsorption of Formaldehyde and Water Vapors in NaY and NaX Zeolites. *Microporous Mesoporous Mater.* **2019**, *288*, No. 109563.
(20) Okachi, T.; Onaka, M. Formaldehyde Encapsulated in Zeolite: A Long-Lived, Highly Activated One-Carbon Electrophile to Carbonyl-Ene Reactions. *J. Am. Chem. Soc.* **2004**, *126* (8), 2306−2307.
(21) Vikrant, K.; Cho, M.; Khan, A.; Kim, K.-H.; Ahn, W.-S.; Kwon, E. E. Adsorption Properties of Advanced Functional Materials against Gaseous Formaldehyde. *Environ. Res.* **2019**, *178*, 108672.
(22) Pei, J.; Zhang, J. S. On the Performance and Mechanisms of Formaldehyde Removal by Chemi-Sorbents. *Chemical Engineering Journal* **2011**, *167* (1), 59−66.
(23) Krishnamurthy, A.; Thakkar, H.; Rownaghi, A. A.; Rezaei, F. Adsorptive Removal of Formaldehyde from Air Using Mixed-Metal Oxides. *Ind. Eng. Chem. Res.* **2018**, *57* (38), 12916−12925.
(24) Vikrant, K.; Kim, K.; He, C.; Giannakoudakis, D. A. Harnessing Adsorption−Catalysis Synergy: Efficient Oxidative Removal of Gaseous Formaldehyde by a Manganese Dioxide/Metal−Organic Framework Nanocomposite at Room Temperature. *Adv. Funct Mater.* **2022**, *32* (22), 2107922.
(25) Gelles, T.; Krishnamurthy, A.; Adebayo, B.; Rownaghi, A.; Rezaei, F. Abatement of gaseous volatile organic compounds: A material perspective. *Catalysis Today* **2020**, *350*, 3−18.
(26) Krishnamurthy, A.; Adebayo, B.; Gelles, T.; Rownaghi, A.; Rezaei, F. Abatement of gaseous volatile organic compounds: A process perspective. *Catalysis Today* **2020**, *350*, 100−119.
(27) Fan, H.; Lakey, P. S. J.; Frank, E. S.; Tobias, D. J.; Shiraiwa, M.; Grassian, V. H. Comparison of the Adsorption−Desorption Kinetics of Limonene and Carvone on TiO_2 and SiO_2 Surfaces under Different Relative Humidity Conditions. *J. Phys. Chem. C* **2022**, *126* (50), 21253−21262.
(28) Wang, C.; Han, Z.; Zou, X.; Liu, H.; Wang, H.; Shu, D.; Chen, T.; Suib, S. L. Ultrathin MnO_2-Coated FeOOH Catalyst for Indoor Formaldehyde Oxidation at Ambient Temperature: New Insight into Surface Reactive Oxygen Species and In-Field Testing in an Air Cleaner. *Environ. Sci. Technol.* **2022**, *56* (15), 10963−10976.
(29) Adebayo, B. O.; Trautman, J.; Al-Naddaf, Q.; Rownaghi, A. A.; Rezaei, F. Passive Control of Indoor Formaldehyde by Mixed-Metal Oxide Latex Paints. *Environ. Sci. Technol.* **2021**, *55* (13), 9255−9265.
(30) Sapsanis, C.; Omran, H.; Chernikova, V.; Shekhah, O.; Belmabkhout, Y.; Buttner, U.; Eddaoudi, M.; Salama, K. N. Insights on Capacitive Interdigitated Electrodes Coated with MOF Thin Films: Humidity and VOCs Sensing as a Case Study. *Sensors (Switzerland)* **2015**, *15* (8), 18153−18166.
(31) ALOthman, Z. A. A Review: Fundamental Aspects of Silicate Mesoporous Materials. *Materials* **2012**, *5* (12), 2874−2902.
(32) Thommes, M.; Kaneko, K.; Neimark, A. V.; Olivier, J. P.; Rodriguez-Reinoso, F.; Rouquerol, J.; Sing, K. S. W. Physisorption of Gases, with Special Reference to the Evaluation of Surface Area and Pore Size Distribution (IUPAC Technical Report). *Pure and applied chemistry* **2015**, *87* (9−10), 1051−1069.
(33) Loparo, J. J.; Roberts, S. T.; Tokmakoff, A. Multidimensional Infrared Spectroscopy of Water. II. Hydrogen Bond Switching Dynamics. *J. Chem. Phys.* **2006**, *125* (19), No. 194522.
(34) Johnson, S. L.; Rumon, K. A. Infrared Spectra of Solid 1:1 Pyridine-Benzoic Acid Complexes; the Nature of the Hydrogen Bond as a Function of the Acid-Base Levels in the Complex1. *J. Phys. Chem.* **1965**, *69* (1), 74−86.
(35) Park, E. J.; Lee, J. H.; Kim, K.-D.; Kim, D. H.; Jeong, M.-G.; Kim, Y. D. Toluene Oxidation Catalyzed by NiO/SiO_2 and NiO/TiO_2/SiO_2: Towards Development of Humidity-Resistant Catalysts. *Catal. Today* **2016**, *260*, 100−106.
(36) Nomura, A.; Jones, C. W. Airborne Aldehyde Abatement by Latex Coatings Containing Amine-Functionalized Porous Silicas. *Ind. Eng. Chem. Res.* **2015**, *54* (1), 263−271.
(37) Broekhuis, R. R.; Lynn, S.; King, C. J. Recovery of Propylene Glycol from Dilute Aqueous Solutions via Reversible Reaction with Aldehydes. *Ind. Eng. Chem. Res.* **1994**, *33* (12), 3230−3237.
(38) Guo, J.; Luo, Y.; Lua, A. C.; Chi, R.; Chen, Y.; Bao, X.; Xiang, S. Adsorption of Hydrogen Sulphide (H_2S) by Activated Carbons Derived from Oil-Palm Shell. *Carbon N Y* **2007**, *45* (2), 330−336.
(39) Zou, J.; Rezaee, R.; Liu, K. Effect of Temperature on Methane Adsorption in Shale Gas Reservoirs. *Energy Fuels* **2017**, *31* (11), 12081−12092.
(40) Wang, Q.; Liu, Y.; Chen, J.; Du, Z.; Mi, J. Control of Uniform and Interconnected Macroporous Structure in PolyHIPE for Enhanced CO_2 Adsorption/Desorption Kinetics. *Environ. Sci. Technol.* **2016**, *50* (14), 7879−7888.
(41) Johnson, M. D.; Weber, W. J. Rapid Prediction of Long-Term Rates of Contaminant Desorption from Soils and Sediments. *Environ. Sci. Technol.* **2001**, *35* (2), 427−433.
(42) Wang, M.; Hong, X.; Chen, J.; Li, J.; Chen, X.; Mi, J.; Liu, Z.; Xiong, S. Two-Step Hydrothermal Synthesis of Highly Active MnO_x-CeO_2 for Complete Oxidation of Formaldehyde. *Chemical Engineering Journal* **2022**, *440*, 135854.
(43) Gu, D.; Sun, W.; Han, G.; Cui, Q.; Wang, H. Lithium Ion Sieve Synthesized via an Improved Solid State Method and Adsorption Performance for West Taijinar Salt Lake Brine. *Chemical Engineering Journal* **2018**, *350*, 474−483.
(44) Kutluay, S. Excellent Adsorptive Performance of Novel Magnetic Nano-Adsorbent Functionalized with 8-Hydroxyquinoline-5-Sulfonic Acid for the Removal of Volatile Organic Compounds (BTX) Vapors. *Fuel* **2021**, *287*, No. 119691.
(45) Liu, Y.; Tian, T. Fabrication of Diatomite/Silicalite-1 Composites and Their Property for VOCs Adsorption. *Materials* **2019**, *12* (4), 551.
(46) Márquez, A.; Berger, T.; Feinle, A.; Hüsing, N.; Himly, M.; Duschl, A.; Diwald, O. Bovine Serum Albumin Adsorption on TiO_2

https://doi.org/10.1021/acsaenm.3c00194
ACS Appl. Eng. Mater. 2023, 1, 1843−1855

Colloids: The Effect of Particle Agglomeration and Surface Composition. *Langmuir* **2017**, *33* (10), 2551−2558.
(47) Kim, H.-J.; Phenrat, T.; Tilton, R. D.; Lowry, G. V. Fe0 Nanoparticles Remain Mobile in Porous Media after Aging Due to Slow Desorption of Polymeric Surface Modifiers. *Environ. Sci. Technol.* **2009**, *43* (10), 3824−3830.
(48) Wang, X.; Ma, X.; Song, C.; Locke, D. R.; Siefert, S.; Winans, R. E.; Möllmer, J.; Lange, M.; Möller, A.; Gläser, R. Molecular Basket Sorbents Polyethylenimine−SBA-15 for CO_2 Capture from Flue Gas: Characterization and Sorption Properties. *Microporous Mesoporous Mater.* **2013**, *169*, 103−111.
(49) Li, X.; Yuan, J.; Du, J.; Sui, H.; He, L. Functionalized Ordered Mesoporous Silica by Vinyltriethoxysilane for the Removal of Volatile Organic Compounds through Adsorption/Desorption Process. *Ind. Eng. Chem. Res.* **2020**, *59* (8), 3511−3520.
(50) Choi, Y.; Cho, W.; Ozaki, A.; Lee, H. Influence of the Moisture Driving Force of Moisture Adsorption and Desorption on Indoor Hygrothermal Environment and Building Thermal Load. *Energy Build* **2021**, *253*, No. 111501.
(51) Nomura, A.; Jones, C. W. Enhanced Formaldehyde-vapor Adsorption Capacity of Polymeric Amine-incorporated Aminosilicas. *Chemistry−A European Journal* **2014**, *20* (21), 6381−6390.
(52) Zhu, J.; Chen, J.; Zhuang, P.; Zhang, Y.; Wang, Y.; Tan, H.; Feng, J.; Yan, W. Efficient Adsorption of Trace Formaldehyde by Polyaniline/TiO2 Composite at Room Temperature and Mechanism Investigation. *Atmos Pollut Res.* **2021**, *12* (2), 1−11.
(53) Yang, Z.; Miao, H.; Rui, Z.; Ji, H. Enhanced formaldehyde removal from air using fully biodegradable chitosan grafted *β*-Cyclodextrin adsorbent with weak chemical interaction. *Polymers* **2019**, *11* (2), 276.
(54) Vikrant, K.; Kim, K.-H.; Kwon, E. E.; Boukhvalov, D. W. Reactive Adsorption and Catalytic Oxidation of Gaseous Formaldehyde at Room Temperature by a Synergistic Copper-Magnesium Bimetal Oxide Biochar Composite. *Chemical Engineering Journal* **2022**, *433*, No. 133497.

https://doi.org/10.1021/acsaenm.3c00194
ACS Appl. Eng. Mater. 2023, 1, 1843−1855